A molecular view of shock interactions and reflections with implications in gas-phase detonations

Amitesh S. Jayaraman, Ethan S. Genter, Hai Wang
Department of Mechanical Engineering, Stanford University
Stanford, CA 94305, USA

1 Introduction

The propagation of confined gas-phase detonations involves interactions and reflections of shocks with other shocks and walls, generating triple points that give rise to the apparent cellular structure of detonations. Triple point collisions are coincident with the birth of detonation cells, and the trajectories of triple points frame the cellular structure [1]. The cellular structure is also strongly modulated by interactions between shocks and the bounding walls [2]. The gas molecules constituting the shock are in a state of non-equilibrium [3, 4] due to the large spatial velocity gradients ($\sim 10^9 - 10^{10}\,\mathrm{s}^{-1}$). Therefore, a local Maxwell-Boltzmann velocity distribution is insufficient to describe the state of the fluid in the shock and the triple point regions. A case in point is the presence of translationally superheated molecules that are emitted ahead of the shock [3] that leads to a substantially skewed local molecular velocity distribution. As a result, computational fluid dynamics (CFD) simulations of gas-phase detonations do not typically account for the impacts of translational non-equilibrium in shock intersections or shock-wall interactions on the local chemical kinetics and hydrodynamics. Recent work has shown that for certain hydrogen-oxygen detonations, the translational non-equilibrium at the shock front and the slow vibrational relaxation following shock compression do not significantly impact chemical kinetics [3, 5]. On the other hand, physics at sub-continuum length scales could influence momentum and energy transfer at larger scales, especially when spatial grid resolution requirements for CFD simulations of gas-phase detonations approach the scale of the local mean free path [6]. In particular, the triple point region, which has a size of the order of the local shock thickness [3] is also the source of the hydrodynamic shear layer that stagnates to form a jet that in turn drives the incipient Mach stem through a virtual piston effect [1]. The strength of the jet depends on the vorticity and energy siphoned from the triple point region and is ultimately influenced by the shear forces and translational non-equilibrium therein. Similarly, the energy transfer between shocks and walls depends on the molecular structure of the shock front and walls and involves non-equilibrium energy transfer mechanisms that are not otherwise observed in gases at local thermal equilibrium.

In the current study, the phenomena of shock Mach reflections and shock-wall energy transfer are studied in detail at the molecular scale to deduce the mechanisms of energy transfer and the impacts of translational non-equilibrium on the local gas dynamics using molecular dynamics (MD) simulations and gas-kinetic theory. We show that molecular momentum and energy transport will be modified beyond the first-order Chapman-Enskog theory of molecular transport [7, 8]. Two cases are considered:

Correspondence to: amiteshs@stanford.edu

(1) the interaction between an inert shock (with normal or tangential incidence) and a specular-elastic and diffuse-inelastic wall, and (2) an inert shock Mach reflection along a specular-elastic wedge that generates triple points. MD simulations are performed for a M $= 5.84$ and M $= 5$ shock propagating in argon (Ar) and nitrogen (N_2) respectively. Energy transfer in both normal and tangential shock-wall interactions occurs primarily by heat conduction; a non-equilibrium ballistic energy transfer mechanism plays a lesser but not insignificant role, particularly in tangential shock incidence. In the early periods of Mach reflection ($\sim$ 500 ps) along a wedge, a high effective vorticity ($\sim 10^{10}$ s^{-1}) shear layer emanates from the triple point region and produces a jet that convects gas at a speed almost equal to that of the Mach stem. The triple point region is characterized and observed to be in a state of translational non-equilibrium where the Chapman-Enskog theory of molecular transport is no longer applicable.

2 Methods

MD simulations were performed in LAMMPS [9] using the velocity-Verlet integrator in a microcanonical (NVE) ensemble. The shock on one end was generated by a piston moving at a constant speed that was supersonic relative to the quiescent gas (either Ar or N_2) at 300 K and at 5 atm pressure. At these conditions, the shock thicknesses were 37 nm for the N_2 shock and 73 nm for the Ar shock, which are approximately 3-5 mean free paths of the pre-shock quiescent gas. A simulation was carried out similar to that in [3] but for a longer (1.3 μm) wedge for the N_2 shock. Consistent with [3], N_2 was modeled using an atom-specific Lennard-Jones potential [10]. The nitrogen triple bond was modeled as a harmonic bond with vibrational frequency 2330 cm^{-1} [11] and N_2 was assumed to be fully vibrationally and rotationally excited ($\gamma = 9/7$). In the simulation of shock reflection, a 35° ideal, reflective wedge was constructed to allow the shock to undergo a Mach reflection.

In the simulations of shock-wall interactions, two types of wall models were considered: (a) a specular-elastic wall and, (b) a diffuse-inelastic wall. Molecules that collide with a specular-elastic wall conserve kinetic energy upon collision thereby establishing the limit of zero energy transfer to the wall. On the other hand, molecules that collide with a diffuse-inelastic wall will lose energy to the wall and will accommodate to the wall temperature T_{wall}. These molecules are then desorbed without any "memory" of their initial momentum or energy before collision. The velocity $\mathbf{c}$ of desorbed molecules of mass m is distributed according to the half Maxwell-Boltzmann distribution at T_{wall},

$$f_{\text{HMB}}(\mathbf{c}) = \begin{cases} 2n\left(m/2\pi k_B T_{\text{wall}}\right)^{3/2} \exp\left(-mv^2/2k_B T_{\text{wall}}\right), \mathbf{c}\cdot\mathbf{n} \leq 0 \\ 0, \mathbf{c}\cdot\mathbf{n} > 0 \end{cases}, \tag{1}$$

where n is the local number density of the molecules and $\mathbf{n}$ is the outward-pointing normal vector of the wall. The limits of a specular-elastic and a diffuse-inelastic wall therefore bracket the range of possible steady gas molecule-surface energy transfer mechanisms, and were implemented in MD simulations of normal shock reflection from a wall (with $\mathbf{n}$ parallel to the shock propagation direction) and tangential shock interaction (with $\mathbf{n}$ orthogonal to the shock propagation direction).

3 Results and Discussion

3.1 Shock Mach Reflection

Fig. 1a shows the pressure distribution obtained from a MD simulation of the Mach reflection of the N_2 shock along the wedge, observed 500 ps after reflection. A distinctive triple point structure is observed, along with an increase in pressure when moving upstream from the Mach stem, indicating a piston effect

on the Mach stem [1]. Fig. 1b shows the triple point region colored by the local tangential velocity (i.e., velocity magnitude parallel to the wedge) highlighting the formation of a nascent jet to the right of the stagnation point of the shear layer. No vortex was observed, in contrast to the vortices observed in CFD simulations at much later stages of Mach stem development [1]. The shear layer and nascent jet are expected to ultimately evolve into the vortex ring-jet complex that further accelerates the jet and drives the Mach stem.

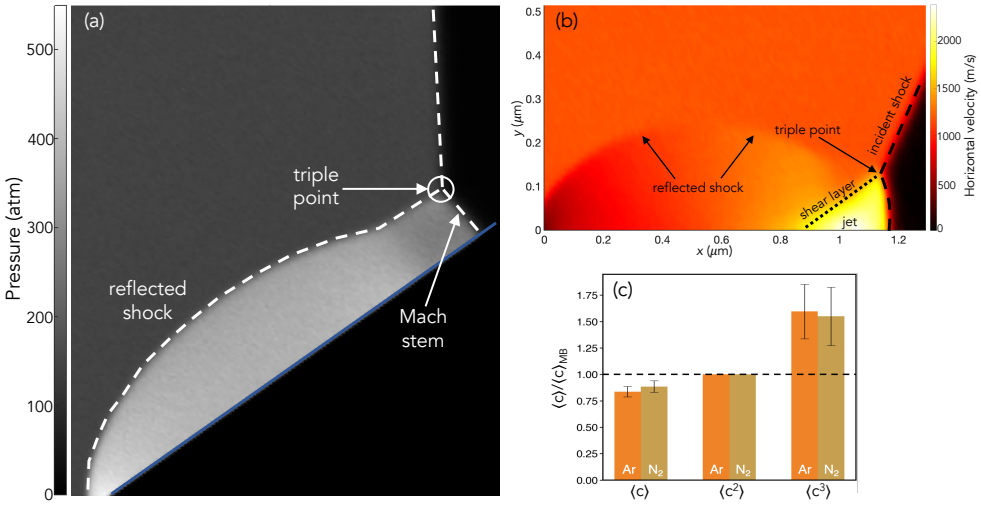

Figure 1: (a) The pressure field of the triple point structure obtained from the MD simulation of a Mach reflection of an M $= 5.00$ N_2 shock on a wedge. (b) Distribution of the local tangential velocity in the vicinity of the triple point, revealing a high-speed jet behind the Mach stem and a shear layer emanating from the triple point. (c) Deviation of the velocity distribution from local equilibrium and a first-order Chapman-Enskog expansion indicating the degree of non-equilibrium [3].

The Navier-Stokes equations cannot be used to describe the region associated with the shock and triple points due to significant translational non-equilibrium as demonstrated in Fig. 1c [3]. The moments of speed in the non-equilibrium distribution relative to that for a Maxwell-Boltzmann distribution, i.e., the deviation of $\langle c^n \rangle / \langle c^n \rangle_{\mathrm{MB}}$ from unity, were used as measures of translational non-equilibrium in [3]. Indeed, $\langle c^n \rangle / \langle c^n \rangle_{\mathrm{MB}} = 1$ also holds true for the first-order Chapman-Enskog perturbation of the local Maxwell-Boltzmann distribution that results in the Newton's law of viscosity and Fourier's law of heat conduction. Therefore, the large deviation of $\langle c^n \rangle / \langle c^n \rangle_{\mathrm{MB}}$ from unity also indicates that the first-order Chapman-Enskog perturbation is no longer applicable within the shock and triple point regions. Consequently, descriptions of molecular energy and momentum transport within the shock and triple point regions require modification beyond the Chapman-Enskog theory.

3.2 Shock-wall interactions

Energy transfer between the shock or hot post-shock flow to a wall is typically modeled using Fourier heat conduction through a thermal boundary layer using a Chapman-Enskog thermal conductivity for the gas. Setting aside the difficulties in numerically resolving the boundary layer [6], the large temperature gradients in the shock region may also limit the applicability of Fourier's law of heat conduction. Furthermore, Fourier conduction neglects the energy transferred to the wall during shock impact. Fig. 2A shows the temperature field of a normal shock propagating at M = 5.84 from left to right through quiescent Ar encountering a fixed wall. The one-dimensional temperature and pressure profiles can be

extracted from the MD simulations (i.e., from the diffuse-inelastic wall simulation and the specular-elastic wall simulation, respectively) before the shock reflects from the wall (Figs. 2B1, C1), during reflection (Figs. 2B2, C2) and after reflection (Figs. 2B3, C23). The diffuse-inelastic wall is an energy sink and slows down the reflected shock. The weaker reflected shock is not sufficiently strong to slow down the flow to stagnation, unlike the case for the specular-elastic shock-wall interaction, creating a velocity boundary layer that grows normally from the wall. Due to the fixed wall temperature, a thermal boundary layer also develops (manifest in the reduction in temperature and pressure close to the wall).

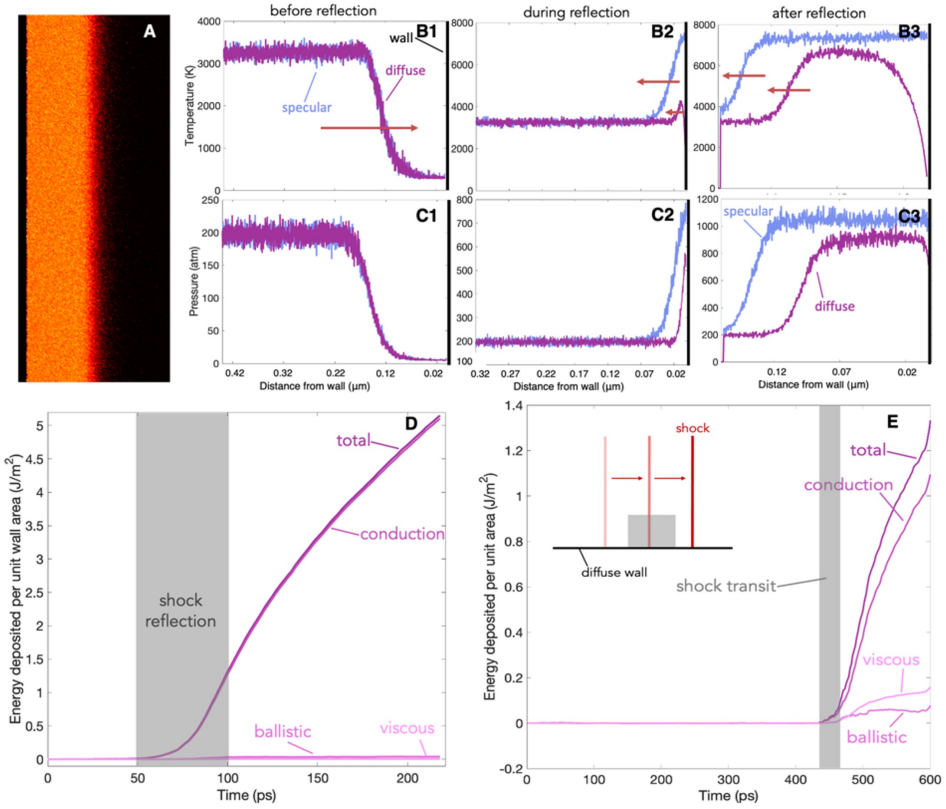

Figure 2: (A) Temperature field of a M = 5.84 Ar shock propagating from left to right from MD simulations, (B1-B3) temperature profiles of a normal shock reflecting from a diffuse-inelastic wall and a specular-elastic wall, (C1-C3) pressure profiles of a normal shock reflecting from a diffuse-inelastic wall and a specular-elastic wall, (D) energy transfer to the diffuse-inelastic wall in normal shock incidence comparing conductive, viscous and ballistic modes and (E) energy transfer to the diffuse-inelastic wall in tangential shock-wall interaction.

The different mechanisms of energy transfer to the wall can be determined from the MD simulations using molecular phase space information. For gas that has a local number density of n and is convecting with a mean velocity of $\mathbf{V}$, the velocity of the individual molecules is given by $\mathbf{v}_i = \mathbf{V} + \mathbf{c}_i$ where $\mathbf{c}_i$ is the peculiar velocity of a molecule i (i.e., $\langle \mathbf{c} \rangle = \sum_{i=1}^{N} \mathbf{c}_i / N = \mathbf{0}$ for an ensemble of N molecules). Note that for molecules of mass m the local effective translational temperature Θ is defined by $\Theta = m\langle c^2 \rangle / 3k_B$. Thus, the heat flux by conduction is given by

$$\mathbf{q}_{\text{cond}} = \frac{1}{2} mn \langle c^2 \mathbf{c} \rangle \tag{2}$$

because only the random thermal motion, rather than a directed or convective motion, of molecules results in conductive heat transfer. Convective motion leads to ballistic energy transfer, whose contribution

is

$$\mathbf{q}_{\text{ballistic}} = mn\left(\frac{1}{2}V^2 + \frac{\gamma R\Theta}{\gamma - 1}\right)\mathbf{V}. \tag{3}$$

The heat flux from viscous work is

$$\mathbf{q}_{\text{viscous}} = mn\langle \mathbf{c}c_x\rangle V_x + mn\langle \mathbf{c}c_y\rangle V_y + mn\langle \mathbf{c}c_x\rangle V_z - mnR\Theta\mathbf{V}, \tag{4}$$

and the sum of $\mathbf{q}_{\text{viscous}} + \mathbf{q}_{\text{ballistic}} + \mathbf{q}_{\text{cond}}$ yields the total heat flux:

$$\mathbf{q}_{\text{tot}} = \frac{1}{2}mn\langle v^2\mathbf{v}\rangle.$$

These formulations of heat flux apply in both equilibrium and non-equilibrium conditions, provided that there are sufficient molecules to ensure that the local average $\langle\cdots\rangle$ is a meaningful quantity. From the MD simulations, we observe that the conductive heat transfer contributes the largest to the energy transfer to the wall for both normal (Fig. 2D) and tangential (Fig. 2E) shock incidence. However, we must distinguish $\mathbf{q}_{\text{cond}}$ in Eq. 2 from Fourier heat conduction. The Chapman-Enskog thermal conductivity of Ar [8] evaluated at the post-shock gas temperature (3271 K) is approximately $k = 0.051$ W/mK. The spatial effective temperature gradient across the shock is approximately 4×10^{10} K^{-1}, resulting in an equivalent Fourier conductive flux of $q_{\text{cond}} = 2.1 \times 10^9$ W/m^2. However, for normal shock incidence (Fig. 2D) we see that the average conductive heat flux during shock reflection is an order of magnitude larger at $\sim 10^{10}$ W/m^2 implying that the effective thermal conductivity is larger than the value obtained from Chapman-Enskog theory for the gas at the post-shock state. The large spatial effective temperature and velocity gradients modify the local molecular velocity distribution by introducing a pronounced high-speed tail [3] that introduces a non-equilibrium conductive heat transfer mechanism that has a significantly larger heat flux than Fourier conduction. In the case of tangential shock incidence (Fig. 2E), the rate of energy transfer is significantly lower but with a larger contribution from viscous energy transfer due to the formation of boundary layers behind the shock.

3.3 Conclusions

MD simulations of shock reflection and shock-wall interactions were conducted to characterize the translational non-equilibrium in the shock and triple point regions. In the simulations of the shock Mach reflection, it was observed that within 500 ps after Mach reflection, a jet of high-speed gas is formed from the shear layer emanating from the triple point region. This jet will subsequently influence Mach stem propagation and the growth of detonation cells [1]. In the study of shock-wall interactions, the large spatial velocity and effective temperature gradients within the shock increased the local effective thermal conductivity beyond that expected from Chapman-Enskog theory, thereby enhancing energy transfer to the wall. The non-equilibrium coupling between high-speed convective flow and molecular transport has implications in the early stages of the detonation cell formation following triple point collision, where local gas dynamics in the shock and triple point regions become relevant. Accurate modeling of these non-equilibrium phenomena at walls and triple point regions will be necessary, especially as the spatial and temporal resolutions for CFD simulations of gas-phase detonations approach molecular scales.

3.4 Acknowledgments

The work was supported by Air Force Office of Scientific Research, United States under Grant FA9550-20-1-0398 managed by Dr. Chiping Li, and by the Office of Naval Research, United States under Grant N00014-22-1-2606 managed by Dr. Steven Martens. ESG acknowledges support by the National

Science Foundation Graduate Research Fellowship under Grant No. DGE-1656518. Some of the computing for this project was performed on the Sherlock cluster at Stanford University. The authors thank Stanford University and the Stanford Research Computing Center for providing computational resources and support that contributed to these research results.

References

[1] P. A. Meagher, X. Shi, A. S. Jayaraman, N. Kateris, X. Zhao, and H. Wang, "The Hydrodynamic Origin of the Detonation Cell", In: 29th International Colloquium on the Dynamics of Explosions and Reactive Systems (ICDERS), SNU Siheung, Korea, 270 (2023).

[2] J. Crane, J. T. Lipkowicz, X. Shi, I. Wlokas, A. M. Kempf, and H. Wang, "Three-dimensional detonation structure and its response to confinement", Proc. Combust. Inst. 39 (3) (2023) 2915-2923.

[3] A. S. Jayaraman, E. S. Genter, W. Dong, and H. Wang, "Collision enhancement in shocks and its implication on gas-phase detonations: A molecular dynamics and gas-kinetic theory study", Proc. Combust. Inst., 40 (1-4) (2024) 105741.

[4] R. Murugesan, and M. Radulescu. "The influence of non-equilibrium translational effects on reactive dynamics during shock to detonation transition using molecular dynamics", In: 29th International Colloquium on the Dynamics of Explosions and Reactive Systems (ICDERS), SNU Siheung, Korea, 274 (2023).

[5] X. Shi, A. S. Jayaraman, and H. Wang, "Probing vibrational nonequilibrium in detonations with ozone", Proc. Combust. Inst. 40 (1-4) (2024) 105695.

[6] P. A. Meagher, and X. Zhao, "Grid resolution considerations for simulating non-ideal cellular detonations", Proc. Combust. Inst. 40 (1-4) (2024) 105412.

[7] W.G. Vincenti, and C.H. Kruger Jr., Introduction to Physical Gas Dynamics, Wiley, New York, 1967.

[8] J.O. Hirschfelder, C.F. Curtiss, and R.B. Bird, The Molecular Theory of Gases and Liquids, John Wiley & Sons, 1964.

[9] A.P. Thompson, H.M. Aktulga, R. Berger, D.S. Bolintineanu, W.M. Brown, P.S. Crozier, P.J. In 't Veld, A. Kohlmeyer, S.G. Moore, T.D. Nguyen, R. Shan, M.J. Stevens, J. Tranchida, C. Trott, and S.J. Plimpton, "LAMMPS - a flexible simulation tool for particle-based materials modeling at the atomic, meso, and continuum scales", Comput. Phys. Commun. 271 (2022) 108171.

[10] J.-P. Bouanich, "Site-site Lennard-Jones potential parameters for N_2, O_2, H_2, CO and CO_2, J. Quant. Spectrosc. Radiat. Transfer 47 (4) (1992) 243–250.

[11] NIST Computational Chemistry Comparison and Benchmark Database, NIST Standard Reference Database Number 101 Release 22, May 2022, Editor: Russell D. Johnson III, http://cccbdb.nist.gov/